Breakup of ^{17}F on ^{208}Pb near the Coulomb barrier

J. F. Liang, J. R. Beene, A. Galindo-Uribarri, J. Gomez del Campo, C. J. Gross, P. A. Hausladen, P. E. Mueller,
D. Shapira, D. W. Stracener, and R. L. Varner
Physics Division, Oak Ridge National Laboratory, Oak Ridge, Tennessee 37831

J. D. Bierman
Physics Department AD-51, Gonzaga University, Spokane, Washington 99258-0051

H. Esbensen
Physics Division, Argonne National Laboratory, Argonne, Illinois 60439

Y. Larochelle
Department of Physics and Astronomy, University of Tennessee, Knoxville, Tennessee 37966

Angular distributions of oxygen produced in the breakup of ^{17}F incident on a ^{208}Pb target have been measured at angles from 75° to 113° and 39° to 79° for beam energies of 98 and 120 MeV, respectively. The data are dominated by the proton stripping mechanism and are well reproduced by dynamical calculations. The measured breakup cross section is approximately a factor of 3 less than that of fusion at 98 MeV. The influence of breakup on fusion is discussed.

I. INTRODUCTION

The study of nuclear reactions near the Coulomb barrier involving loosely bound nuclei has received considerable attention in recent years. This is primarily driven by the advent of radioactive ion beams [1]. It is frequently observed in stable beam experiments that the subbarrier fusion cross sections are enhanced over one-dimensional barrier penetration model predictions. The enhancement can be described by channel couplings, where the interplay of the intrinsic degrees of freedom and reaction channels modify the single barrier to multiple barriers [2]. The barriers appearing at lower energies are responsible for the fusion enhancement. Breakup is a major reaction channel in the scattering of loosely bound nuclei; this removal of the incident flux would lead to fusion suppression [3,4]. On the other hand, the coupling to the breakup channel can change the barrier distribution which could result in fusion enhancement [5]. Experimental efforts have been put forward to study the influence of breakup on subbarrier fusion [1].

The fusion excitation functions of the neutron skin nucleus ^{6}He on ^{209}Bi [6–8] and ^{238}U [9] were measured, and large subbarrier fusion enhancements were observed in both cases. The breakup cross sections of ^{6}He on ^{209}Bi measured below the Coulomb barrier are orders of magnitude greater than fusion [10,11]. Measurements with stable ^{9}Be, which has a neutron binding energy of 1.665 MeV, on ^{208}Pb [12] and ^{209}Bi [13,14] found that the fusion was not enhanced below the Coulomb barrier and was suppressed by about 30% above the barrier. In the ^{9}Be+^{208}Pb reaction, the incomplete fusion reaction $\alpha+^{208}$Pb following the breakup of ^{9}Be into $n+\alpha+\alpha$ was observed. The suppression of fusion at energies above the barrier was attributed to the projectile breakup. The barrier distribution extracted from the fusion excitation functions is consistent with a single barrier

for the ^{9}Be+^{208}Pb and ^{9}Be+^{209}Bi [15], even though very large breakup yields were observed below the barrier [15]. The fusion of ^{9}Be+^{209}Bi was compared to that of ^{11}Be (a neutron halo nucleus with neutron binding energy of 0.504 MeV) +^{209}Bi. At energies below the barrier, the cross sections were similar to that of ^{9}Be+^{209}Bi, whereas at energies above the barrier, the cross sections are significantly larger than the predictions from a coupled-channels calculation which takes into account the large rms radius of ^{11}Be. However, the precision of the data was not very good and further measurements are required [15].

On the proton rich side, fusion of a proton drip line nucleus, ^{17}F, with ^{208}Pb was measured [16]. The fusion excitation function is almost identical to that of ^{16}O+^{208}Pb and ^{19}F+^{208}Pb after correcting for the Coulomb barrier arising from the charge and size differences. There was no enhancement or perhaps a small suppression of fusion below the barrier. It is noted that the loosely bound proton can be polarized in the large Coulomb field of the target in such a way that the proton is shielded by the core and the breakup probability is reduced [17,18]. This paper reports the breakup of ^{17}F on ^{208}Pb measured near the Coulomb barrier.

II. EXPERIMENT

The experiment was carried out at the Holifield Radioactive Ion Beam Facility, where the isotope separator on-line technique was employed for radioactive ion beam production. A 44 MeV deuteron beam from the Oak Ridge isochronous cyclotron was incident on a fibrous hafnium oxide target to produce short-lived ^{17}F by the ^{16}O$(d,n)^{17}$F reaction [19]. The reaction products were extracted from a closely coupled kinetic ejection negative ion source [20], mass analyzed, and accelerated by the 25 MV tandem electrostatic accelerator. The ^{17}O isobar was removed from the acceler-

ated beams by inserting an 80 μg/cm^2 carbon foil at the exit of the tandem accelerator and selecting the 9^+ ions with a 90° analyzing magnet. The beam intensity was measured by detecting the secondary electrons generated during transmission of the beam through a 10 μg/cm^2 carbon foil with a microchannel plate detector. The average intensity was 1.5 $\times 10^6$ and 8×10^6 ^{17}F^{9+}/s for the 98 and 120 MeV reactions, respectively. The highest intensity achieved was 10^7 ions/s for the 120 MeV beam.

The target used was a self-supporting ^{208}Pb foil with a nominal thickness of 1.8 mg/cm^2. The reaction energies, 98 and 120 MeV, were calculated for the beams at the middle of the target by taking into account the energy loss in the target. The reaction products were detected by a ΔE-E telescope composed of a 29 μm Si detector mounted in front of a 1000 μm double-sided silicon strip detector (DSSD). The area of the Si detector and the DSSD is 5×5 cm^2. The DSSD, which has 16 vertical and 16 horizontal strips, was placed at 10.5 cm from the target and symmetric with respect to the horizontal plane, i.e., half of the detector above and half of the detector below the plane. The detector telescope was arranged to face the center of the target. For the 98 MeV measurement, the center of the ΔE-E telescope was set at 74.5° and 100° and the target was turned 20° and 45°, respectively, with respect to the beam and toward the detectors. Events collected in pixels on the same vertical strip were binned together to obtain the angular distribution. For the measurement at 120 MeV beam energy, the center of the ΔE-E telescope was placed at 44.5° and 69.5°. The target was perpendicular to the beam for the former and turned 15° with respect to the beam for the latter. At forward angles, $\theta_{lab} < 57°$, pixels on the same vertical strip have to be divided into two groups, eight middle pixels and eight outer pixels, in order to keep the angular spread similar to the backward angles ($\simeq 2°$). At backward angles, the variation of scattering angle for pixels on a vertical strip is small. Events in pixels on the same vertical strip can be summed to increase statistics. The uniformity of the Si detector was determined by measuring elastic scattering at forward angles. The position of the elastically scattered particles penetrating the detector was obtained from the overlap of the horizontal and vertical strips of the DSSD. The energy loss of the elastically scattered particles in the 256 (16×16) pixels was compared to kinematics and stopping power calculations. Two 50 mm^2 Si surface barrier detectors placed at 10° on either side of the beam were used to monitor the beam position and for normalization between runs. The absolute cross section was obtained by normalizing the yields to the 10° Si detectors, where the elastic scattering was taken as Rutherford scattering. Because of the detector telescope spanning a total of 26°, the target thickness for particles detected in different angles was taken into account for deducing cross sections.

An E versus ΔE plot for the 120 MeV ^{17}F-induced reaction is displayed in Fig. 1. It is obtained by summing events in the pixels of one vertical strip at $\theta_{lab} = 65°$. The energy loss ΔE was corrected for the nonuniformity of the Si detec-
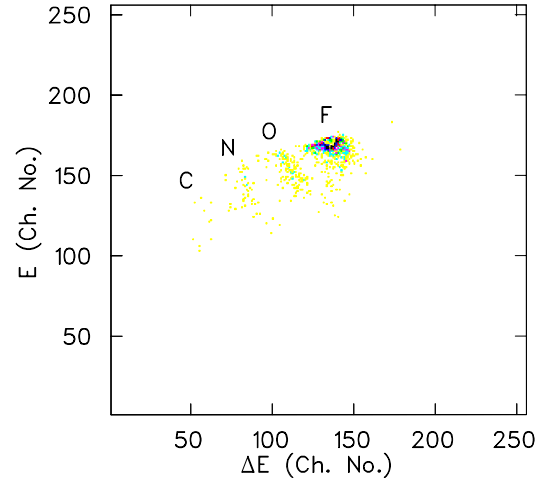

FIG. 1. Histogram of E vs ΔE for reaction products produced in 120 MeV ^{17}F$+^{208}$Pb measured at $\theta_{lab} = 65°$ by summing events in a vertical strip of the DSSD.

tor. A group of oxygen events can be clearly identified and is well separated from the elastically scattered ^{17}F.

III. RESULT AND DISCUSSION

The angular distributions of oxygen produced in ^{17}F $+^{208}$Pb collisions at 98 and 120 MeV are shown in Figs. 2 and 3, respectively. The angular distributions are bell shaped and have a peak near 95° for the 98 MeV reaction and 57° for the 120 MeV reaction. Since the ΔE-E telescope is not able to resolve mass, calculations were performed to estimate contributions of reactions leading to oxygen isotopes other than ^{16}O. The charge exchange reaction (^{17}F,^{17}O) has a Q-value of -0.11 MeV. Two-step distorted wave born approximation (DWBA) calculations using the code FRESCO [21] were performed to estimate the contribution of this reaction. Sequential single-nucleon transfer reactions, ^{17}F $\rightarrow ^{16}$O$\rightarrow ^{17}$O and ^{17}F$\rightarrow ^{18}$F$\rightarrow ^{17}$O, were calculated. In the calculations, transfer to excited states in the projectilelike and targetlike nuclei were included. States that have large spectroscopic factors measured in light ion transfer reactions
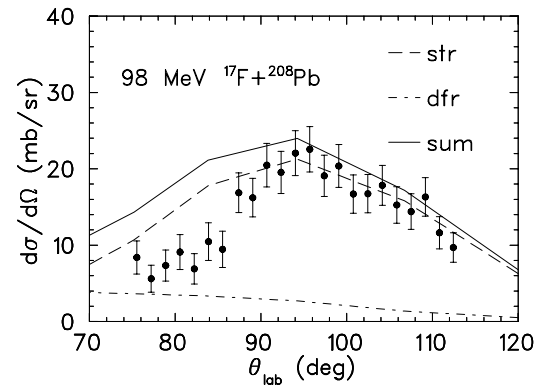

FIG. 2. Angular distribution of oxygen produced from 98 MeV ^{17}F$+^{208}$Pb. The calculated stripping and diffraction breakup are shown by the dashed and dash-dotted curves, respectively. The solid curve is for the sum of the two.
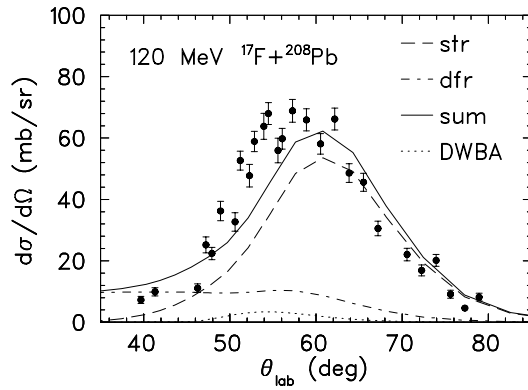
FIG. 3. Angular distribution of oxygen produced from 120 MeV ^{17}F+^{208}Pb. The calculated stripping and diffraction breakup are shown by the dashed and dash-dotted curves, respectively. The solid curve is for the sum of the two. The results of one-step DWBA transfer calculations are shown by the dotted curve.

or large cross sections calculated in one-step single-nucleon transfer reactions, were selected for the two-step DWBA calculations. Table I presents the states included in the calculations. In these calculations, the spectroscopic factors were set to 1.0 to estimate the magnitude of the yields. The shape of the calculated (^{17}F,^{17}O) angular distribution at E_{lab} =120 MeV is similar to the measured angular distribution and has a peak at θ_{lab}=58°. However, the calculated peak cross section is 0.0028 mb/sr which is several orders of magnitude less than the measured value. Although reactions leading to ^{18}O and ^{207}Bi in the exit channel have positive Q-values, they cannot occur by simple single-step transfer processes. Therefore, the cross sections are expected to be smaller than that for one-proton transfer [22]. The results of DWBA calculations for one-step proton transfer ^{208}Pb(^{17}F,^{16}O)^{209}Bi at 120 MeV are shown by the dotted curve in Fig. 3. One proton transfer to the six lowest single particle states in ^{209}Bi was calculated by the code PTOLEMY [23], with the spectroscopic factors set to 1.0. It can be seen that neither one-proton transfer nor charge exchange can ac-

TABLE I. States included in calculations of the (^{17}F, ^{17}O) reaction by successive nucleon transfer.

Nucleus	E^* (MeV)	J^π
^{16}O	0.0	0^+
^{18}F	0.0	1^+
	0.937	3^+
^{17}O	0.0	$\frac{5}{2}^+$
	0.871	$\frac{1}{2}^+$
^{209}Bi	0.0	$\frac{9}{2}^-$
	0.896	$\frac{7}{2}^-$
	1.609	$\frac{13}{2}^+$
^{207}Pb	0.0	$\frac{1}{2}^-$
^{208}Bi	0.0	5^+
	0.063	4^+
	0.937	3^+
	1.034	4^+

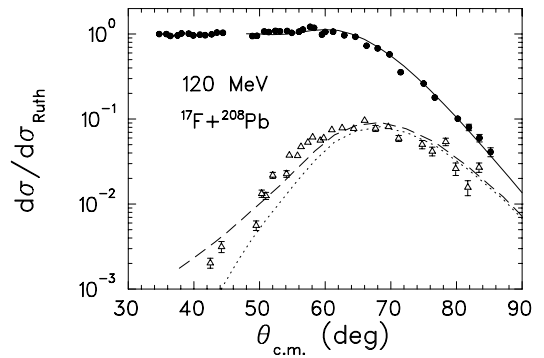FIG. 4. Angular distribution of elastic scattering (filled circles) in 120 MeV ^{17}F+^{208}Pb. The result of an optical model fit to the data is shown by the solid curve. The angular distribution of oxygen produced in the same reaction is presented for comparison (open triangles). The calculated stripping is shown by the dotted curve and the sum of stripping and diffraction breakup is shown by the dashed curve.

count for the measured oxygen angular distribution. Since the direct charge exchange is orders of magnitude smaller than that of one-nucleon transfer [24], its contribution to the data can be safely ignored.

The measured angular distributions are compared to results of dynamical calculations, where the relative motion of the proton and the ^{16}O core is described quantum mechanically by solving the time dependent Schrödinger equation for the two-body breakup in the Coulomb and nuclear fields from the target nucleus [25]. It has been shown that calculations of this kind are suitable for energies near the Coulomb barrier [26]. The time evolution of the projectile wave function was calculated to obtain the angular distribution of ^{16}O from the ^{17}F→^{16}O+p reaction. The breakup angular distribution is obtained by multiplying the breakup probability calculated as a function of impact parameter by a fit to the measured elastic scattering cross section at the corresponding Rutherford scattering angle. The measured angular distribution of elastic scattering at 120 MeV is shown in Fig. 4. Since the angular resolution is ∼2° and the cross sections fall off exponentially at large angles, exponential functions fitted between two adjacent data points were used to calculate the weighted average of each data point at large angles. The solid curve shows an optical model fit to the elastic scattering, which is used in converting calculated breakup probabilities into an angular distribution. The resulting breakup cross section is shown by the dashed curve in Fig. 4. The dotted curve is the separate contribution from stripping, which dominates the breakup and is in fairly good agreement with the measurement shown by the open triangles.

The calculated breakup cross section is compared to the measured angular distribution of oxygen fragments in Figs. 2 and 3, for 98 and 120 MeV, respectively. The dashed curve is the stripping and the dash-dotted curves is the diffraction dissociation, and their sum is shown by the solid curve. It can be seen that the measured angular distribution is predominantly due to the stripping breakup reaction. The agreement between the data and calculations is very good for the 98 MeV measurement. For the 120 MeV reaction, the mea-
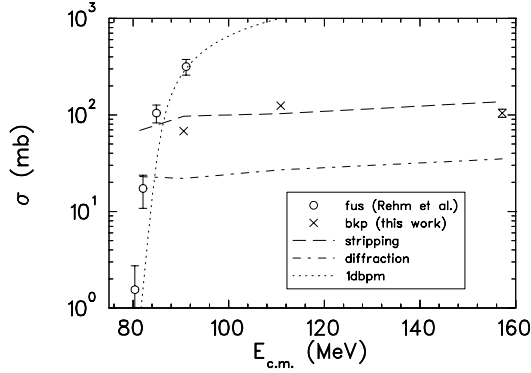
FIG. 5. Comparisons of the fusion excitation function ($\bigcirc$) of ^{17}F+^{208}Pb measured by Rehm *et al.* [16] and angle-integrated breakup cross sections measured in this work ($\times$). The data point at $E_{cm}=157.2$ MeV is obtained from Ref. [27]. The dotted curve is the one-dimensional barrier penetration model prediction and the dashed and dash-dotted curves are for stripping and diffraction breakup, respectively, predicted by dynamical calculations.
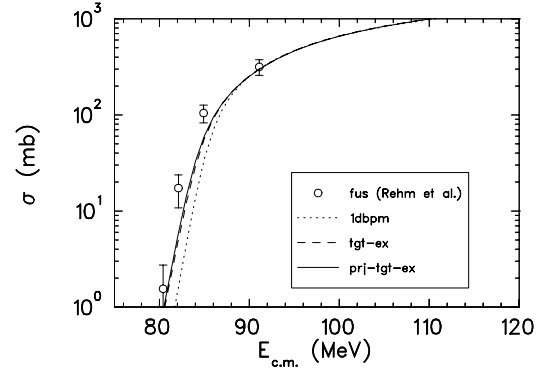

FIG. 6. Fusion excitation function for ^{17}F+^{208}Pb predicted by a one-dimensional barrier penetration model (dotted curve), coupled-channels calculations taking into account target excitations (dashed curve), and projectile and target excitations (solid curve) as described in the text.

sured angular distribution is shifted slightly forward compared to the calculated distribution but the total cross sections are in good agreement (see Fig. 5).

The angular distributions of oxygen were fit to the Gaussian function to obtain angle integrated breakup cross sections, as shown in Table II. Figure 5 displays the fusion excitation function measured by Rehm *et al.* [16] and the breakup cross sections measured in this work and Ref. [27]. The calculated diffraction and stripping breakup are shown by the dash-dotted and dashed curves, respectively. As it was seen in the angular distribution of oxygen fragments that the measured breakup is dominated by proton stripping, the angle integrated breakup cross sections are in good agreement with the calculated stripping cross sections. Near the barrier, the diffraction breakup is a factor of 3 less than stripping which, in turn, is about a factor of 3 less than fusion.

The result of a one-dimensional barrier penetration model calculation for ^{17}F+^{208}Pb using the code CCMOD [28] is shown in Figs. 5 and 6 by the dotted curve. The barrier potential parameters, $V_0=235.5$ MeV, $r_0=1.1$ fm, and $a=0.65$ fm, were taken from the analysis of fusion measurements of a neighboring system, ^{16}O+^{208}Pb [29], since the excitation function is almost identical to that of ^{17}F+^{208}Pb after correcting for the Coulomb barrier. As can be seen, the calculation underpredicts the cross sections at subbarrier energies. Coupled-channels calculations were performed with the code CCMOD using procedures employed for analysis of the ^{16}O+^{208}Pb measurement in Ref. [29]. It is well established that inelastic excitations of the projectile and target can contribute to subbarrier fusion enhancement. In many cases, coupling to inelastic excitation channels can account

for the enhanced fusion rates. Calculations including the excitation of ^{208}Pb to the lowest 2^+, 3^-, and 5^- states were carried out. Furthermore, it was found in the analysis of the ^{16}O+^{208}Pb data that the coupling of double-phonon excitations is essential for reproducing the barrier distribution. The coupling of two-phonon states $3^-\otimes3^-$ in the harmonic limit and all the resulting cross coupling terms, e.g., $3^-\otimes5^-$ were considered in the calculations. The result is shown by the dashed curve in Fig. 6. The calculation still underpredicts the measurement. The first excited state of ^{17}F is bound by 105 keV and can be excited from the ground state with a large B(E2) value, B(E2)$\downarrow=63.4$ e^2 fm^4 [30,31]. The results of coupled-channels calculations including the excitation of ^{17}F is shown by the solid curve in Fig. 6. It can be seen that the increase in the subbarrier cross sections is very small when this projectile excitation is included and the coupled-channels calculations still underpredict the subbarrier cross sections.

In the fusion of ^{16}O+^{208}Pb, the excitation function was reproduced by calculations coupling to the inelastic excitation channels only. Since all the Q-values for neutron transfer are negative, it is not necessary to consider transfer in the coupled-channels calculations. The neutron transfer Q-values in ^{17}F+^{208}Pb are positive for up to six-neutron pickup. In particular, the two- and four-neutron transfer have Q-values greater than 5 MeV. This can be compared to ^{40}Ca+^{90}Zr and ^{40}Ca+^{96}Zr, where very large subbarrier fusion enhancement was observed in the latter [32]. Coupling to the inelastic excitations of projectile and target only reproduces the ^{40}Ca+^{90}Zr measurement. There are still large discrepancies between the measured cross sections of ^{40}Ca+^{96}Zr and the coupled-channels calculations. The major difference in the two reactions is neutron transfer. The Q-values for multineutron transfer are negative in ^{40}Ca+^{90}Zr, but positive in ^{40}Ca+^{96}Zr. Measurements of transfer near the barrier found large cross sections for the ^{96}Zr target [33]. The influence of transfer on fusion is demonstrated in a semiclassical model calculation [33–35], where the fusion cross sections as well as transfer for ^{40}Ca+^{96}Zr are reproduced. Figure 7 presents the results of coupled-channels calculations includ-

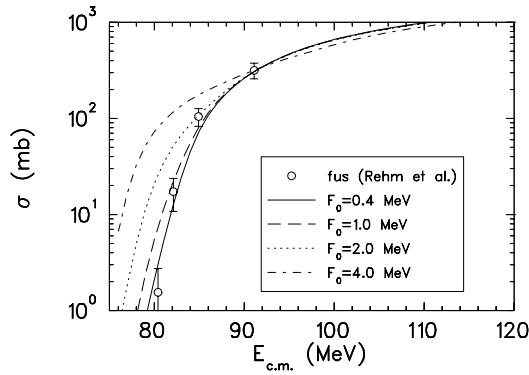TABLE II. Angle integrated stripping cross sections for ^{17}F+^{208}Pb.

E_{lab} (MeV)	98	120	170 [27]
σ (mb)	68±5	125±7	104±10

FIG. 7. Results of coupled-channels calculations including inelastic excitations and transfer in ^{17}F+^{208}Pb. The results for transfer coupling constant $F_0 = 0.4$, 1.0, 2.0, and 4.0 MeV are shown by the solid, dashed, dotted, and dash-dotted curves, respectively.
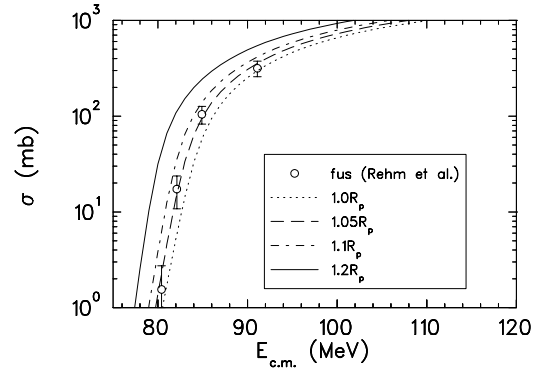

FIG. 8. Results of coupled-channels calculations including only inelastic excitations (dotted curve) and the radius of the projectile increased by 5% (dashed curve), 10% (dash-dotted curve), and 20% (solid curve).

ing the inelastic excitations, discussed above, and nucleon transfer. The transfer is treated approximately in the code CCMOD, therefore, only qualitative comparison can be made here. The transfer form factor is given by

$$F(r) = \frac{F_0}{\sqrt{4\pi}} \exp\left[-\frac{(r - R_1 - R_2)}{a}\right] \text{ MeV,}$$

where F_0 is the coupling constant, $R_{1,2}$ are the nuclear radii, and $a = 1.2$ fm is the diffuseness parameter. The solid, dashed, dotted, and dash-dotted curves are for coupling constant $F_0 = 0.4$, 1.0, 2.0, and 4.0 MeV, respectively. To simplify the calculation, three channels, one-proton stripping, one-neutron pickup, and two-neutron pickup, were included. The fusion excitation function can be reasonably reproduced with F_0 set between 0.4 and 1 MeV. However, it is noted that the quantity F_0 can be as large as 3 or 4 MeV depending on the transferred angular momentum and the orbitals occupied by the transferred nucleons [28,32,36]. Based on the calculations presented in Fig. 7, the fusion excitation function can be reproduced by including transfer of up to two nucleons in the calculations with the coupling constant $F_0 \lesssim 1$ MeV. If channels of transferring more than two nucleons are included and $F_0 > 1$ MeV is used, the calculation will overpredict the measured cross sections, i.e., the fusion is suppressed below the barrier. To better account for the influence of transfer on fusion in ^{17}F+^{208}Pb, measurements of multinucleon transfer and more sophisticated model calculations such as in Ref. [33] are required. Up to now, one of the reactions which has not been considered in the calculations is breakup. The simplified coupled-channels code used here cannot treat breakup rigorously. Nevertheless, it is conceivable that if fusion is suppressed, breakup can be responsible.

It has been reported that the ^{17}F has a large rms radius, $\langle r \rangle_{rms} = 3.7$ fm [37]. In the coupled-channels calculations, the nuclear radius is given by $r_0 A^{1/3}$, where $r_0 = 1.1$ fm is the radius parameter and A is the mass number. The effect of the large rms radius of ^{17}F was not accounted for in the previous calculations. To explore these effects, the radius parameter of the projectile was adjusted in the calculations. Since the treatment of coupling to transfer degrees of freedom has

large uncertainties introduced by the coupling constant F_0, only inelastic excitations were included. In Fig. 8, the dashed, dash-dotted, and solid curves are for increasing the radius of ^{17}F by 5%, 10%, and 20%, respectively. It can be seen that the fusion excitation function can be well reproduced by increasing the radius of ^{17}F by 5%, whereas increasing the radius by 10% results in a calculated cross section that exceeds the measurements. If transfer channels were included, the discrepancy would be larger. This further suggests that the fusion of ^{17}F and ^{208}Pb may be suppressed.

In the ^{9}Be+^{208}Pb reaction, complete fusion was found to be suppressed at energies above the barrier. However, the sum of complete and incomplete fusion agrees with a coupled-channels calculation. The discrepancy between the measured complete fusion cross sections and the coupled-channels prediction is attributed to the breakup of ^{9}Be [12]. The incomplete fusion arises from ^{9}Be breaking up into two α particles and a neutron, and subsequently, an α particle fuses with the target. The fusion measurements of ^{17}F on ^{208}Pb in Ref. [16] are made by detecting fission fragments, and therefore, probably determine total fusionlike cross section (complete + incomplete fusion) rather than the complete fusion cross section since the incomplete fusion reaction, ^{16}O+^{208}Pb, produces fission events very similar to those of the complete fusion reaction. Consequently, it is not known whether the complete fusion of ^{17}F+^{208}Pb is suppressed above the barrier. Measurements of ^{17}F on ^{208}Pb at 10 MeV/nucleon showed that it is necessary to consider core absorption (^{16}O absorbed by ^{208}Pb) in the dynamical calculation to reproduce the measured diffraction breakup yield [27]. The dynamical calculations presented in Figs. 2 and 3 also include core absorption. It is expected that incomplete fusion is present in ^{17}F+^{208}Pb. A coincidence measurement of the breakup proton and the fission fragments are required to identify the incomplete fusion reaction.

The predicted diffraction breakup of ^{17}F→^{16}O+p seems too small to influence fusion significantly. However, the stripping breakup yield is about one-third of fusion. The energy dependence of this reaction predicted by the dynamical calculation, is presented by the dashed curve in Fig. 5. The calculated stripping cross section exceeds that for fusion be-

low the barrier. The measured breakup of ^{6,7}Li and ^{9}Be in the vicinity of the barrier in ^{6,7}Li$+^{208}$Pb [38] and ^{9}Be $+^{209}$Bi [15], respectively, shows similar behavior. The analysis of elastic scattering of ^{6}Li$+^{208}$Pb in Ref. [39] shows that the imaginary potential increases as the energy decreases below the barrier and the threshold anomaly [40] disappears. Because of this strong absorption, the enhancement of fusion at low energies should be small and the breakup reaction is expected to be strong [39]. The measured fusion yields for ^{17}F$+^{208}$Pb were not enhanced and perhaps even slightly suppressed below the barrier. It is conceivable that strong absorption exists resulting in large stripping breakup that removes ^{17}F from the fusion channel. It would be interesting to measure the elastic scattering and study the energy dependence of the interaction potentials.

Large subbarrier fusion enhancement and transfer/breakup were observed in the ^{6}He$+^{209}$Bi reaction [7,10]. Analysis of elastic scattering indicated an absence of the threshold anomaly [11]. In this case, the strong absorption may not enhance fusion much but may contribute mostly to transfer/ breakup, as pointed out in Ref. [39]. The neutron binding energy of ^{6}He is fairly low. As suggested in Ref. [7], the large subbarrier fusion enhancement may arise from neutron flow since the threshold barrier correlates with neutron binding energies [41]. In the ^{17}F$+^{208}$Pb reaction, the proton binding energy is very low but the proton flow must be strongly suppressed because of the Coulomb barrier. Therefore, the behavior of fusion below the barrier is different from that of ^{6}He$+^{209}$Bi.

IV. SUMMARY AND CONCLUSION

The breakup of 98 and 120 MeV ^{17}F on ^{208}Pb was measured by detecting oxygen in singles. The angular distributions of oxygen are well reproduced by dynamical calcula-

tions and found to be dominated by stripping breakup. Near the barrier, the angle integrated stripping cross section is about 30% of that of fusion. It has been shown in the analysis of ^{6}Li$+^{208}$Pb elastic scattering that the imaginary potential continues to be large below the barrier. In this case, the breakup yields are large, but fusion is not much enhanced because the threshold anomaly is absent. This may explain why a subbarrier fusion enhancement was not observed in ^{17}F$+^{208}$Pb. Simplified coupled-channels calculations were performed to explore the effects of coupling to both inelastic excitations and transfer degrees of freedom on fusion. Furthermore, the radius of ^{17}F was adjusted in the calculations to study the change in the fusion excitation function. The results suggest that fusion may be suppressed at energies below the barrier. In contrast, large subbarrier fusion enhancements were observed for fusion of the neutron skin nucleus ^{6}He on ^{209}Bi and ^{238}U. Further experiments are required to examine whether the differences observed between the ^{6}He- and ^{17}F-induced fusion are due to breakup or other reaction mechanisms. Measurements using neutron halo nuclei, such as ^{11}Be and ^{11}Li, and proton halo nuclei, such as ^{8}B and ^{26}P, would provide useful additional information.

[1] C. Signorini, Nucl. Phys. **A693**, 190 (2001), and references therein.

[2] M. Dasgupta, D.J. Hinde, N. Rowley, and A.M. Stefanini, Annu. Rev. Nucl. Part. Sci. **48**, 401 (1998).

[3] M.S. Hussein, M.P. Pato, L.F. Canto, and R. Donangelo, Phys. Rev. C **46**, 377 (1992).

[4] N. Takigawa, M. Kuratani, and H. Sagawa, Phys. Rev. C **47**, R2470 (1993).

[5] C.H. Dasso and A. Vitturi, Phys. Rev. C **50**, R12 (1994).

[6] J.J. Kolata *et al.*, Phys. Rev. C **57**, R6 (1998).

[7] J.J. Kolata *et al.*, Phys. Rev. Lett. **81**, 4580 (1998).

[8] P.A. De Young *et al.*, Phys. Rev. C **58**, 3442 (1998).

[9] M. Trotta *et al.*, Phys. Rev. Lett. **84**, 2342 (2000).

[10] E.F. Aguilera *et al.*, Phys. Rev. Lett. **84**, 5058 (2000).

[11] E.F. Aguilera *et al.*, Phys. Rev. C **63**, 061603(R) (2001).

[12] M. Dasgupta *et al.*, Phys. Rev. Lett. **82**, 1395 (1999).

[13] A. Yoshida *et al.*, Phys. Lett. B **389**, 457 (1996).

[14] C. Signorini *et al.*, Eur. Phys. J. A **2**, 227 (1998).

[15] C. Signorini, Eur. Phys. J. A **13**, 129 (2002).

[16] K.E. Rehm *et al.*, Phys. Rev. Lett. **81**, 3341 (1998).

[17] H. Esbensen and G.F. Bertsch, Nucl. Phys. **A600**, 37 (1996).

[18] H. Esbensen and G.F. Bertsch, Nucl. Phys. **A706**, 383 (2002).

[19] R.F. Welton *et al.*, Nucl. Instrum. Methods Phys. Res. B **159**, 116 (1999).

[20] G.D. Alton, Y. Liu, C.W. Williams, S.N. Murray, Nucl. Instrum. Methods Phys. Res. B **170**, 515 (2000).

[21] I.J. Thompson, Comput. Phys. Rep. **7**, 167 (1988).

[22] D. G. Kovar, in *Proceedings of the International Conference on Reactions between Complex Nuclei*, edited by R.L. Robinson, F.K. McGowan, J.B. Ball, and J.H. Hamilton (North-Holland, Amsterdam 1974).

[23] M.H. Macfarlane and S.C. Pieper, Report No. ANL-76-11 Rev. 1, 1978 (unpublished).

[24] H.H. Duhm, H. Hafner, R. Renfordt, M. Goldschmidt, O. Dragun, and K.-I. Kubo, Phys. Lett. **48B**, 1 (1974).

[25] H. Esbensen, G.F. Bertsch, and C.A. Bertulani, Nucl. Phys. **A581**, 107 (1995).

[26] H. Esbensen and G.F. Bertsch, Phys. Rev. C **59**, 3240 (1999).

[27] J.F. Liang *et al.*, Phys. Rev. C **65**, 051603(R) (2002).

[28] M. Dasgupta, A. Navin, Y.K. Agarwal, C.V.K. Baba, H.C. Jain,

M.L. Jhingan, and A. Roy, Nucl. Phys. **A539**, 351 (1992).

[29] M. Dasgupta, K. Hagino, C.R. Morton, D.J. Hinde, J.R. Leigh, N. Takigawa, H. Timmers, and J.O. Newton, J. Phys. G **23**, 1491 (1997).

[30] P.M. Endt, At. Data Nucl. Data Tables **23**, 3 (1979).

[31] B.A. Brown, B.H. Wildenthal, W. Chung, S.E. Massen, M. Bernas, A.M. Bernstein, R. Miskimen, V.R. Brown, and V.A. Madsen, Phys. Rev. C **26**, 2247 (1982).

[32] H. Timmers, D. Ackermann, S. Beghini, L. Corradi, J.H. He, G. Montagnoli, F. Scarlassara, A.M. Stefanini, and N. Rowley, Nucl. Phys. **A633**, 421 (1998).

[33] G. Montagnoli, S. Beghini, F. Scarlassara, A.M. Stefanini, L. Corradi, C.J. Lin, G. Pollarolo, and A. Winther, Eur. Phys. J. A **15**, 351 (2002).

[34] A. Winther, Nucl. Phys. **A572**, 191 (1994).

[35] A. Winther, Nucl. Phys. **A594**, 203 (1995).

[36] G. Pollarolo, R.A. Broglia, and A. Winther, Nucl. Phys. **A406**, 369 (1983).

[37] R. Morlock, R. Kunz, A. Mayer, M. Jaeger, A. Müller, J.W. Hammer, P. Mohr, H. Oberhummer, G. Staudt, and V. Kölle, Phys. Rev. Lett. **79**, 3837 (1997).

[38] G.R. Kelly *et al.*, Phys. Rev. C **63**, 024601 (2000).

[39] N. Keeley, S.J. Bennett, N.M. Clarke, B.R. Fulton, G. Tungate, P.V. Drumm, M.A. Nagarajan, and J.S. Lilley, Nucl. Phys. **A571**, 326 (1994).

[40] M.A. Nagarajan, C.C. Mahaux, and G.R. Satchler, Phys. Rev. Lett. **54**, 1136 (1985).

[41] P.H. Stelson, H.J. Kim, M. Beckerman, D. Shapira, and R.L. Robinson, Phys. Rev. C **41**, 1584 (1990).